Transition Strategies for Tilt-Wing Aircraft

Marc May and Daniel Milz and Gertjan Looye

Despite being the critical flight phase for tilt-wings, the transition maneuver is still not well understood with respect to aerodynamics and flight dynamics. Flight and handling qualities in this regime are primarily defined by the size and shape of the transition corridor, which describes physical limitations and other boundaries. Typically, the corridor is obtained based on static trim analysis, which results in a conservative estimate that neglects the dynamic maneuverability of the aircraft. As a first fundamental step for the determination of the full transition corridor, this paper presents a comprehensive dynamic analysis of the longitudinal tilt-wing transition, considering various operational strategies for the maneuver. The analysis is based on an optimal control approach where the dynamic control problem is transcribed into a nonlinear programming (NLP) problem. The developed framework successfully explores different regions of the transition corridor by adapting constraints and objective functions, and thereby lays the foundation for future determination of transition boundaries. The optimized trajectories show that the phenomena of transition folds found in static analyses are damped within dynamic investigations. Furthermore, the re-transition maneuver proves to be more challenging from a flight physics perspective because of high effective angles of attack, and requires upward motion to avoid flow separation.

May, Marc and Milz, Daniel and Looye, Gertjan (2024) Transition Strategies for Tilt-Wing Aircraft. In: AIAA Scitech 2024 Forum, 2024. AIAA Scitech 2024 Forum, 8-12 Jan 2024, Orlando, FL. DOI: 10.2514/6.2024-2189

Transition Strategies for Tilt-Wing Aircraft

Marc May*, Daniel Milz† and Gertjan Looye‡
Institute of System Dynamics and Control, German Aerospace Center (DLR), 82234 Weßling, Germany

Despite being the critical flight phase for tilt-wings, the transition maneuver is still not well understood with respect to aerodynamics and flight dynamics. Flight and handling qualities in this regime are primarily defined by the size and shape of the transition corridor, which describes physical limitations and other boundaries. Typically, the corridor is obtained based on static trim analysis, which results in a conservative estimate that neglects the dynamic maneuverability of the aircraft. As a first fundamental step for the determination of the full transition corridor, this paper presents a comprehensive dynamic analysis of the longitudinal tilt-wing transition, considering various operational strategies for the maneuver. The analysis is based on an optimal control approach where the dynamic control problem is transcribed into a nonlinear programming (NLP) problem. The developed framework successfully explores different regions of the transition corridor by adapting constraints and objective functions, and thereby lays the foundation for future determination of transition boundaries. The optimized trajectories show that the phenomena of transition folds found in static analyses are damped within dynamic investigations. Furthermore, the re-transition maneuver proves to be more challenging from a flight physics perspective because of high effective angles of attack, and requires upward motion to avoid flow separation.

I. Introduction

TRANSFORMATIONAL aircraft promise to combine the advantages of both fixed- and rotary-wing flight, thereby allowing to establish efficient, flexible, and time-saving transport options for poorly linked regions. The subcategory of tilt-wing aircraft provides efficient cruise flight with low requirements on ground infrastructure. As engines and airfoil stay aligned throughout the flight envelope, slipstream effects can be exploited. At the same time, these vehicles are the most complex configuration when compared to other types of the emerging electric vertical takeoff and landing (eVTOL) fleet. Historical challenges arose from complex mechanical control systems [1], bad handling qualities due to the heterogeneous flight envelope [2, 3], and especially restricted design freedom due to fuel-based propulsion [4, 5]. Today, distributed electric propulsion (DEP) allows for flexible vehicle configurations and recent developments in digitization and automation alleviate limitations of the control system. A remaining challenge is the intuition for and understanding of the flight dynamic behavior, which is characterized by aero-propulsive interactional effects and flow separation. From a flight control perspective, the missing knowledge is circumvented, e.g. in the form of robust [6] or sensor-based [7, 8] control methods. However, in order to derive safe and efficient maneuvers or to determine the safe flight envelope for both nominal and failure case, a better understanding of the dynamic system is required. In a previous work [9], we developed a representative aircraft model covering all relevant effects. The accompanying static trim analysis provided first insights into the transition behavior, but neglected important dynamic characteristics of the system. Therefore, this paper will extend the investigation on tilt-wing transition with a dynamic analysis of different transition strategies, providing the basis for the determination of the dynamic transition corridor.

A. Related Work

Bridging both flight regimes of hover and cruise flight, the transition is the decisive maneuver for tilt-wing aircraft. As these vehicles are not designed for continuous vertical flight, the conversion to cruise conditions is to be performed soon after take-off. In opposite direction, the re-transition is crucial to enable a safe vertical landing. While the behavior in the outer regimes of wing-borne and thrust-borne flight resembles other, more familiar aircraft configurations like airplanes, helicopters and multicopters with well established theory, the transition regime remains subject of research. This is in particular due to its inhomogeneity with rapidly changing flight conditions. In literature, especially the re-transition is

*Research Assistant, marc.may@dlr.de
†Research Assistant, daniel.milz@dlr.de, AIAA member
‡Head of Department, gertjan.looye@dlr.de, AIAA member

highlighted as a challenging maneuver, as the descent flight condition at low thrust setting pushes the effective angle of attack (AoA) towards flow separation [2, 10]. Next to the stall boundary, transition maneuverability is also limited by the thrust range, the tilt angle range, and structural loads [2]. Other boundaries might occur due to control system limitations [11] or physical burden for pilot and passenger. Together, these boundaries form the transition corridor, which gives a good indication for the flying qualities of transformational aircraft [2]. For tilt-wing, the transition corridor is typically defined as the region of usable tilt angle over flight speed. For other transition strategies or aircraft types, the tilt angle might be replaced by the pitch angle or a combination of pitch and tilt angle. To be more general, it could also be replaced by a conversion factor that represents the state between horizontal and vertical flight mode in an intuitive range, e.g. $[0; 1]$. The width of the corridor is directly linked to the handling qualities, as a narrow corridor requires a precise maneuver, resulting in high pilot workload.

The transition corridor is a subregion of the flight envelope and likewise usually determined by a static trim analysis, in either simulation [12, 13], wind tunnel [14, 15] or flight tests [11]. However, this approach ignores the maneuverability of the aircraft [16] and neglects important dynamic effects. For the flight envelope, reachable set theory is used to extend the conservative trim boundaries [16, 17]. It is based on solving optimization problems that take into account the system dynamics. This approach is part of the theory of optimal control (OC), where optimization problems including continuous system dynamics are transcribed to nonlinear programming problems (NLP), which can then be solved for example using Newton-based solvers [18]. The system dynamics are considered in the form of constraints in the NLP formulation. The OC approach was deployed by Doff-Sotta et al. [19], Chauhan and Martins [20], and Panish and Bacic [21] to optimize transition trajectories for tilt-wing aircraft. These works minimize energy demand during transition, or the integral squared thrust as a proxy. Exploiting a priori knowledge of an Air Traffic Control (ATC) provided flight corridor, [19] reformulates the aircraft equation of motion (EoM) in order to obtain an optimization problem that is convex in objective and constraints. Both works consider slipstream interaction in their modeling approach, but otherwise maintain a low complexity, for example consider only translational motion in in 2D flight path coordinates. In contrast, Cook [13] identifies dynamic transition trajectories within the level flight manifold without optimization, but instead using best guess control policies for the tilt angle to minimize unwanted transition effects. All of these research efforts identified single dynamic trajectories for the transition. To the authors knowledge, the transition corridor of tilt-wing aircraft has not yet been determined with a dynamic analysis.

Next to tilt-wings, transition flight has also been investigated for other types of transformational aircraft, and results and findings can be transferred from there. From a flight mechanics perspective, especially tailsitter aircraft are comparable to tilt-wing aircraft. Instead of tilting their wings with respect to the fuselage, the pitch attitude of the complete aircraft is changed to convert from hover to cruise flight. That results in similar effective angles of attack and aero-propulsive interactions as encountered during tilt-wing transition. In contrast to tilt-wings, more literature can be found for tailsitter transition analysis, where most investigations make use of the optimal control approach. While [22] uses a general formulation for the transition, Kubo and Suzuki [24] optimize for different transition strategies and verify them experimentally. Introducing a constraint to avoid flow separation, [23] creates so-called in- and outbound transitions that exploit vertical aircraft motion to maintain low effective AoA. The same maneuvers were proposed in [11] for a tilt-wing aircraft. With the intention of online planning or even control in the form of model predictive control (MPC), [25, 26] use differential flatness properties of the dynamics to reduce the computational cost of the optimization. While the above-mentioned publications were focused on single trajectory optimization, Yang et al. and Zhong and Wang identify dynamic transition corridors. In [27], the corridor is determined by constraints for forces and moments, derived from a set of rules for the respective transition maneuvers, without solving optimization problems. In contrast, [28] creates the dynamic transition corridor as the outer hull of optimal trajectories found by arbitrarily varying initial and final conditions. It is mentioned that this set is still conservative and feasible trajectories might lie outside the boundaries.

B. Scope of the Paper

This paper aims at the dynamic analysis of the longitudinal tilt-wing transition maneuvers for both forward (from hover to cruise) and backward (from cruise to hover) transition. A setup for trajectory optimization in the form of an optimal control problem formulation is implemented. Based on that, different transition strategies with their respective objectives and constraints are investigated and evaluated. With a focus on manned flight, maneuvers with extreme conditions for pilot and passengers are not considered. Other than that, the intention is to include the most relevant transition strategies as a foundation for future transition corridor determination.

II. Optimal Control Framework

The developed optimal control framework is primarily based on the guidelines presented by Betts [18] and was extended with insights into the toolboxes FALCON by TUM [29], and ICLOCS2 by Imperial College London [30]. Like both reference toolboxes, the framework is interfaced with the common solver IPOPT [31], which is based on the interior point method. In the following, first the dynamic model of the tilt-wing is described before transferring it to the optimal control formulation.

A. Tilt-Wing Aircraft

The transition analysis is conducted on a tandem tilt-wing configuration as illustrated in Fig. 1. For a detailed quantitative description, the reader is referred to [9, 32]. The longitudinal motion of the aircraft is of chief interest for the analysis of the transition maneuver. Without failure cases, the aircraft is assumed to be symmetrical with respect to the x-z-plane, wherefore components distributed along the y-axis can be summarized in single 2D components. That accounts for the number of eight propellers and four control surfaces, which are evenly distributed to both wings. Main (rear) wing components are denoted by index 1, while canard (front) wing components are denoted by index 2. Note that these indices consequently deviate from the notation used in [9, 32], where full 6-degree-of-freedom (DoF) motion was considered. The state of each wing is defined by three inputs, the tilt angle δ_w with a range of $[0°; 90°]$ from level to vertical deflection, the control surface deflection δ_e limited to $[-30°; 30°]$ and the thrust T. It is assumed that the maximum thrust of the vehicle equals twice the gravitational force to allow both maneuverability and redundancy in failure cases. That leads to variable ranges for T of $[0\,\mathrm{N}; 4500\,\mathrm{N}]$ for the grouped propellers respectively. For wing dependent variables, the running index i will be used in the following. While both wings have the same NASA GA(W)-2 profile and a rectangular planform, the reference area of the main wing is larger than that of the canard wing. The center of gravity (CG) is slightly shifted towards the rear section. These design choices characterise the pitching moment behavior during the transition.

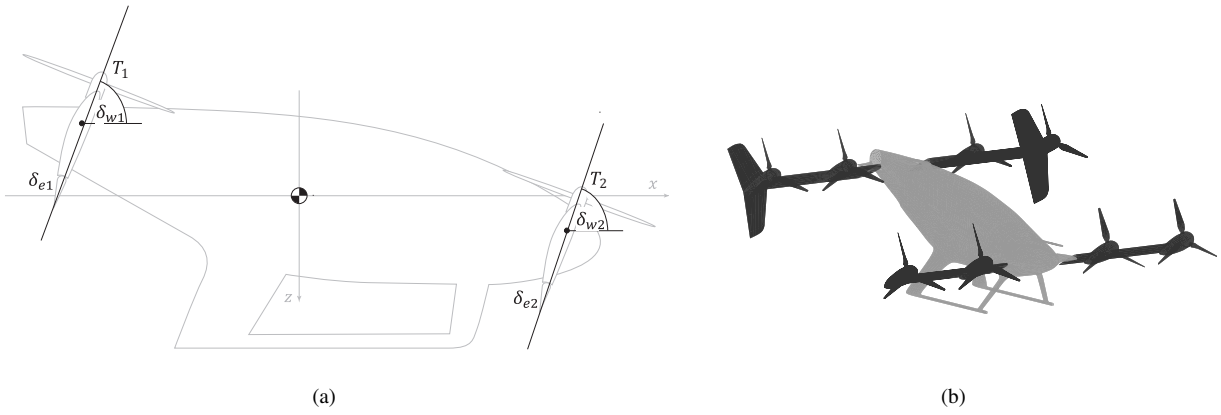

(a) (b)

Fig. 1 Sideview of tandem tilt-wing configuration, (a) in early transition and (b) 3D view in late transition

B. Longitudinal Dynamic Model

To keep the number of optimization variables and thereby the size of the resulting NLP problem small, the lateral motion of the aircraft is neglected and a longitudinal model including pitching motion is implemented. The resulting equations of motion (EOM) can be expressed as:

$$\dot{x}^E = u^B \cos\theta + w^B \sin\theta \tag{1}$$

$$\dot{z}^E = u^B \sin\theta - w^B \cos\theta \tag{2}$$

$$\dot{u}^B = -q w^B - g \sin\theta + \frac{1}{m} \sum_{i=1}^{2} \left(T_i \cos\delta_{w,i} + F^B_{A,x,i} \left(v^B, \delta_{w,i}, T_i, \delta_{e,i} \right) \right) \tag{3}$$

$$\dot{w}^B = qu^B + g\cos\theta + \frac{1}{m}\sum_{i=1}^{2}\left(T_i \sin\delta_{w,i} + F^B_{A,z,i}\left(v^B, \delta_{w,i}, T_i, \delta_{e,i}\right)\right) \tag{4}$$

$$\dot{\theta} = q \tag{5}$$

$$\dot{q} = \frac{1}{I_{\mathrm{yy}}}\left(\sum_{i=1}^{2} \boldsymbol{m}^B_{A,y,i} + T_i l_i\left(\delta_{w,i}\right)\right) \tag{6}$$

where the aircraft position $\boldsymbol{x}^E = \begin{bmatrix} x^E & z^E \end{bmatrix}^{\mathrm{T}}$ is defined in the ENU frame $\mathcal{F}_E$, while the velocity $\boldsymbol{v}^B = \begin{bmatrix} u^B & w^B \end{bmatrix}^{\mathrm{T}}$ and its derivative is defined in body coordinates $\mathcal{F}_B$. The states for the rotational motion are pitch angle θ and pitch rate q, and the inertia around the y-axis is represented by I_{yy}. The respective thrust forces of main and canard wing have a tilt-angle-dependent lever arm $l_i = f\left(\delta_{w,i}\right)$ to create a control pitching moment. Next to the freestream defined by the body velocity and tilt angle, the thrust induced slipstream and control surface deflections $\delta_{e,i}$ determine the aerodynamic forces $F^B_{A,x,i}$ and $F^B_{A,z,i}$, given in body frame.

Due to the symmetric counter-rotating propeller arrangement with respect to the x-z plane, propeller torque is canceled and can be neglected in the model. Therefore, the commanded thrust $T_{c,i}$ is modelled as a direct input.

Concerning aerodynamics and slipstream interactions, the model used for optimization is a simplified form of the strip-theory model presented in [9]. The effect of slipstream interaction is limited to the axially induced velocity, as radial velocities are assumed to cancel due to symmetry. The tangential swirl velocity is neglected to maintain two-dimensional aerodynamics. Further neglecting lateral inflow, the axially induced slipstream velocity [33] is

$$v_{i,ax} = -\frac{V_{x,i}}{2} + \sqrt{\frac{V^2_{x,i}}{4} + \frac{T_i}{2\rho\pi R_p^2}} \tag{7}$$

where $V_{x,i}$ is the inflow velocity perpendicular to the rotor plane. For fully contracted slipstreams, the induced velocity is twice as high as the velocity in the rotor plane [33]. In [6], it was assumed that the aerodynamic reference point is located at the position of full slipstream contraction. As the slipstream contraction model byMcCormick [34] is a function of geometry parameters (distance between propeller plane and wing reference point $d_{s,i}$, and propeller radius R_p) which remain constant for the tilt-wing, the induced velocity in the aerodynamic reference point can be represented accurately by a constant slipstream contraction factor $s_{\mathrm{sc},i} < 2$, which is different for both wings:

$$s_{\mathrm{sc},i} = 1 + \frac{d_{s,i}/R_p}{\sqrt{1 + \left(d_{s,i}/R_p\right)^2}} \tag{8}$$

$$s_{\mathrm{sc},1} = 1.57 \qquad s_{\mathrm{sc},2} = 1.47 \tag{9}$$

In order to obtain the effective angle of attack α_{eff} at wing i, the effective velocity at the airfoil is calculated by transforming $\boldsymbol{v}^B$ to the wing frame and adding the slipstream induced velocity:

$$\boldsymbol{v}^W_i = \boldsymbol{R}^{WB}_i\left(\delta_{w,i}\right) \cdot \boldsymbol{v}^B + v_{i,ax} \cdot s_{sc,i}\begin{bmatrix} 1 & 0 & 0 \end{bmatrix}^{\mathrm{T}} \tag{10}$$

$$\alpha_{\mathrm{eff},i} = \arctan\left(\frac{v^W_{z,i}}{v^W_{x,i}}\right) \tag{11}$$

$$\{C_L, C_D, C_M\}_i = f\left(\alpha_{\mathrm{eff,i}}\right) \tag{12}$$

with the rotation matrix from body to wing frame $\boldsymbol{R}^{WB}_i$. The effect of body rotational rates on the resulting velocity is neglected, as the effect would be small for realistic rates and the pitch motion is balanced to zero within the optimization.

With the effective angle of attack, the aerodynamic coefficients (compare Eq. (12)) can be computed using the model presented by [35]. To improve performance, the 360° AoA coefficient model can be preprocessed and saved in look-up tables (LUT). As recommended in [18] for improved convergence, tabular data is interpolated using splines to obtain continuous functions up to second order derivatives. The effect of control surface deflection on the aerodynamic coefficients is modelled according to [36] and leads to offsets of the aerodynamic coefficients, see Eq. (14) and Eq. (15). To include the reduced flap effectiveness in post-stall without sacrificing continuity, the offsets due to flap deflections

are faded out with a scaled arctan-function. Furthermore, an elliptic lift distribution is applied to correct the 2D lift coefficient, resulting in

$$C_{L,3D} = C_{L,2D}\frac{\pi}{4} \qquad C_{D,3D} = C_{D,2D} + \frac{C_L^2}{\pi\Lambda_i} \tag{13}$$

with aspect ratio $\Lambda_i = {}^{b_i^2}/_{S_i}$, b_i and S_i being wing span and wing reference area.

The aerodynamic coefficients are defined in the aerodynamic frame and first need to be transformed to the body frame by applying the rotation matrix $\boldsymbol{R}_y\,(\varphi)$ for a rotation around the y-axis. The resulting aerodynamic forces and moments in body frame are:

$$\boldsymbol{f}_{A,i}^B = q_i S_i \boldsymbol{R}_y\left(\alpha_{\text{eff,i}-\delta_{w,i}}\right)\begin{bmatrix} -\left(C_D + \Delta C_{D,\delta_e} + \frac{C_L^2}{\pi\Lambda_i}\right) \\ 0 \\ -\left(C_L + \Delta C_{L,\delta_e}\right)\frac{\pi}{4} \end{bmatrix}_i \tag{14}$$

$$\boldsymbol{m}_{A,i}^B = q_i S_i c_i \begin{bmatrix} 0 \\ C_M \\ 0 \end{bmatrix}_i + \boldsymbol{f}_{A,i}^B \times \boldsymbol{r}_{wb,i}^B \tag{15}$$

Here, c_i is the mean aerodynamic chord and the dynamic pressure is $q_i = {}^1\!/_2\,\rho||\boldsymbol{v}_i^W||^2$, while $\boldsymbol{r}_{wb,i}^B$ describes the position of the wing with respect to the CG.

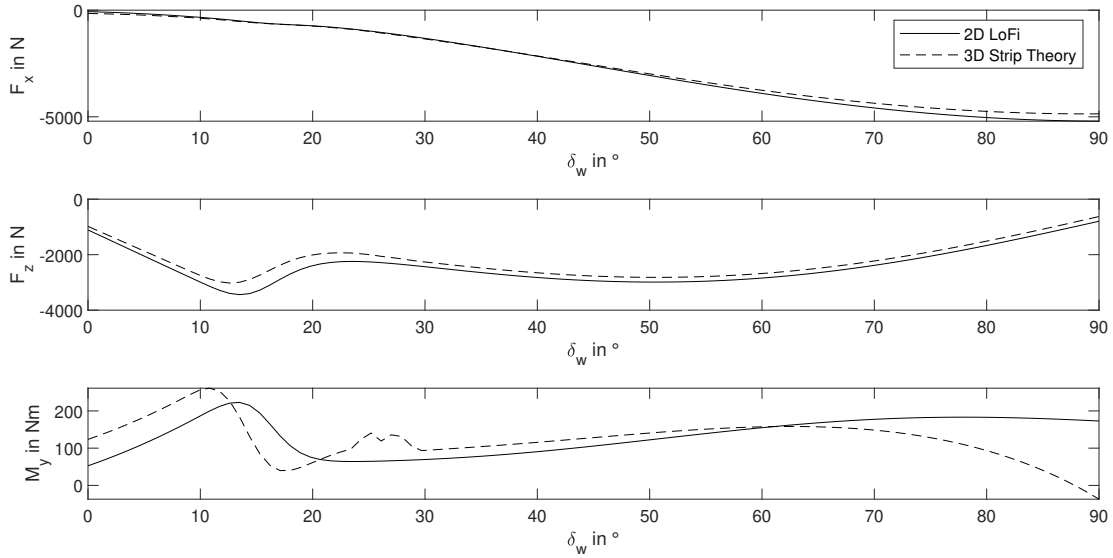

Fig. 2 Comparison of 2D low fidelity and 3D strip theory aerodynamic model for constant axial flight velocity of $V = 25\,\mathrm{m\,s^{-1}}$ and at constant thrust settings of $T_1 = T_2 = 1500\,\mathrm{N}$.

In order to consider actuator dynamics, system inputs are modelled as simple transfer functions or by applying lower and upper rate constraints $u_{\mathrm{rc},l}$ and $u_{\mathrm{rc},u}$ in discrete form [18]:

$$u_{\mathrm{rc},l} \leq \frac{u_{k+1} - u_k}{\Delta\tau \cdot t_f} \leq u_{\mathrm{rc},u} \tag{16}$$

where the central term describes the change of variable u per discrete time step $\Delta\tau \cdot t_f$.

In Fig. 2, the accuracy of the reduced fidelity model for optimal control is compared to the strip theory aerodynamic model presented in [9]. When lateral stabilizers and airfoils on the landing skids (compare Fig. 1(b)) are neglected, both models show good conformance. The differences result chiefly from the effect of induced swirl velocity.

C. Optimal Control Problem Formulation

The aim of an optimal control approach is to find the control vector $u(t) \in \mathbb{R}^{n_u}$ that minimizes a cost function $J : \mathbb{R}^{n_x} \times \mathbb{R}^{n_u} \times \mathbb{R} \to \mathbb{R}$ subject to the dynamics $f : \mathbb{R}^{n_x} \times \mathbb{R}^{n_u} \times \mathbb{R} \to \mathbb{R}^{n_x}$ of a system with states $x(t) \in \mathbb{R}^{n_x}$, while complying with path, boundary and derivative constraint functions (ϕ_g, ϕ_b and ϕ_r). While path constraints limit output variables $y = g(x, u)$, boundary constraints define the initial and final states $x_0 = x(t_0)$ and $x_f = x(t_f)$. The general mathematical formulation of the problem is

$$
\begin{aligned}
\min_{t, x(t), u(t)} \quad & J = \phi_f\left(t_f, x\left(t_f\right), u\left(t_f\right)\right) + \int_{t_0}^{t_f} \phi_t\left(t, x(t), u(t)\right) dt \\
s.t. \quad & \dot{x} = f\left(x(t), u(t)\right) \\
& t_l \le t_f \le t_u \\
& x_l \le x(t) \le x_u \\
& u_l \le u(t) \le u_u \\
& g_l \le \phi_g\left(x(t), u(t)\right) \le g_u \\
& b_l \le \phi_b\left(t_f, x(t_0), x\left(t_f\right)\right) \le b_u \\
& r_l \le \phi_r\left(x(t), u(t)\right) \le r_u
\end{aligned}
\tag{17}
$$

where ϕ_f represents the terminal point cost and ϕ_t is the integral cost, usually used in squared form. All defects imposed by the system dynamics are considered by $\boldsymbol{c} = 0$ in the form $0 \le \boldsymbol{c} \le 0$, whereas path and rate constraints are implemented with their lower and upper boundaries. The initial time t_0 is fixed to zero, while the terminal time t_f is free and part of the optimization problem. Upper and lower limits are indicated by index u and l respectively.

In order to solve the problem with Newton-based methods on a finite set of variables and constraints, the continuous problem is transcribed using a direct collocation method in order to obtain an NLP. Here, direct collocation with the trapezoidal method on a grid with N points is applied. The resulting NLP variables to be optimized are:

$$
\boldsymbol{z} = \left[t_f, x_1, u_1, x_2, u_2, \ldots, x_N, u_N\right]^{\mathrm{T}} \tag{18}
$$

where the indices correspond to the respective time grid point. Eq. (18) shows that the size of the NLP depends on the number of inputs and states describing the dynamic system as well as the temporal discretization. The form of the variable vector z allows to exploit the sparsity pattern of the Jacobian $\boldsymbol{G} \equiv \frac{\partial \boldsymbol{c}}{\partial \boldsymbol{z}}$ and the Hessian of the Lagrangian

$$
\boldsymbol{H}_L = \nabla^2_{zz} L(z) = \nabla^2_{zz} J(z) - \sum_{i=1}^{m} \lambda_i \nabla^2_{zz} \boldsymbol{c}_i(z) \tag{19}
$$

with Lagrange multipliers λ_i, as explained in [18]. Further methods applied to improve accuracy and convergence are scaling of variables and a remesh strategy.

Transferred to the tilt-wing 3-DoF application, the state and input vectors, according to Section II.B, are:

$$
\boldsymbol{x} = \begin{bmatrix} x^E & z^E & u^B & w^B & \theta & q & T_1 & T_2 & \delta_{w1} & \delta_{w2} \end{bmatrix}^{\mathrm{T}} \tag{20}
$$

$$
\boldsymbol{u} = \begin{bmatrix} T_{1,c} & T_{2,c} & \delta_{w1,c} & \delta_{w2,c} & \delta_{e1,c} & \delta_{e2,c} \end{bmatrix}^{\mathrm{T}} \tag{21}
$$

Here, the inputs of thrust T and tilt angle δ_w were modelled as first-order delay elements (time constants $\tau_T = 1/5$ and $\tau_{\delta_w} = 2$) while control surface deflections δ_e are rate limited according to Eq. (16). Table 1 gives an overview on nominal variable bounds and rate constraints. Single variables are then adapted to the respective transition strategy. The constant M is an appropriate large number that represent unboundedness. Maximum accelerations in $\mathcal{F}_B$ are given as ratios of gravitational acceleration g and are adopted from values for nominal takeoff and landing maneuvers of commercial airliners. In addition to the first-order delay behavior of thrust and pitch angle, the commanded inputs are smoothened using additional rate constraints. As the exploration space of the IPOPT solver is not hard-limited by the variable boundaries, the lower bound for the thrust is increased from 0 to 1 in order to avoid complex results in Eq. (7).

The optimized transition trajectory leads the aircraft from hover (x_h) to cruise (x_c) conditions or vice versa. Considering the state variables, the hover flight state is defined by zero body velocities $u^B = w^B = 0$ and a high tilt angle $\delta_{w,i,\text{hover}} = \{\delta_{w,i} \mid 80° \le \delta_{w,i} \le 90°\}$, while cruise conditions imply zero vertical velocity $w^B = 0$ but a horizontal

Table 1 State and input variables of the optimal control problem and their respective boundaries and rate constraints.

State Variables					
Variable	Unit	lower Bound	upper Bound	lower Rate Constraint	upper Rate Constraint
x^E	m	0	M	0	100
z^E	m	$-M$	M	−50	50
u^B	$\mathrm{m\,s^{-1}}$	0	100	$-0.5g$	$0.5g$
w^B	$\mathrm{m\,s^{-1}}$	−50	50	$-0.25g$	$0.25g$
θ	°	−0.5	0.5	$-M$	M
q	$^\circ\,\mathrm{s^{-1}}$	$-1e^{-2}$	$1e^{-2}$	$-M$	M
T_1	N	1	4500	$-M$	M
T_2	N	1	4500	$-M$	M
$\delta_{w,1}$	°	0	90	$-M$	M
$\delta_{w,2}$	°	0	90	$-M$	M
Input Variables					
Variable	Unit	lower Bound	upper Bound	lower Rate Constraint	upper Rate Constraint
$T_{1,c}$	N	1	4500	$-M$	M
$T_{1,c}$	N	1	4500	$-M$	M
$\delta_{w1,c}$	°	0	90	−45	45
$\delta_{w2,c}$	°	0	90	−45	45
$\delta_{e1,c}$	°	−30	30	−45	45
$\delta_{e2,c}$	°	−30	30	−45	45

velocity $u^B_{\text{cruise}} = \{u^B \mid 40\,\mathrm{m\,s^{-1}} \leq u^B \leq 50\,\mathrm{m\,s^{-1}}\}$ and low tilt angle $\delta_{w,i,\text{cruise}} = \{\delta_{w,i} \mid 0^\circ \leq \delta_{w,i} \leq 10^\circ\}$. Other variable bounds are either consistent with Table 1 or depend on the considered transition strategy. The respective flight states are assigned to the initial and terminal state conditions x_0 and x_f according to the transition direction. The initial and final inputs are found by a trim analysis, $\boldsymbol{u}_0 \in \{\boldsymbol{u} | \dot{\boldsymbol{x}}\,(t_0, \boldsymbol{u}) = 0\}$ and $\boldsymbol{u}_f \in \left\{\boldsymbol{u} | \dot{\boldsymbol{x}}\,\left(t_f, \boldsymbol{u}\right) = 0\right\}$, enforcing both hover and cruise to be equilibrium flight states. In reference literature [21], the importance of the initial guess solution for convergence is highlighted. For the presented setup, it was sufficient to interpolate between initial and final trim state to obtain initial guesses on the discrete time grid. However, the setup makes use of solving a sequence of optimal control problems with increasing complexity and forwarding the solution from one stage to the next. A simple model, neglecting flaps and first-order delay behavior of inputs, is solved first, before the presented "full" problem is warm-started with the solution. This primarily improves computation time, while the standalone "full" problem can likewise be solved directly. A similar positive effect on computation time is observed when the problem is initially solved on a coarse grid and subsequent mesh refinement is applied. Final results are obtained on a grid with $N = 101$ control points.

If not contradicting the desired transition strategy presented in Section III, the following objectives are of interest for the optimization:

- minimize the transition time t_f, as flight within the thrust-based flight regime is energy demanding
- minimize the terminal distance x_f^E, for transition maneuvers in tight spaces
- minimize the terminal altitude, especially for re-transition, as vertical descent is energy demanding
- minimize the offset from a reference trajectory, defined by z_{ref}, for level or glide-path transitions
- minimize the sum of squared integral thrust as an energy equivalent

which results in the following multi-objective cost function.

$$J = w_1\, t_f + w_2\, x_f^E + w_3\, z_f^E \int_0^{t_f} \left[w_4 \left(z^E - z^E_{\text{ref}} \right)^2 + w_5 \left(T_1^2 + T_2^2 \right) \right] dt \tag{22}$$

The weights w_j determine the user-defined importance of single objectives, but are also used to scale all terms to a value close to unity, in order to obtain a well-posed Hessian matrix.

III. Transition Strategies

In this chapter, different strategies for performing the transition maneuver are explained, described mathematically in the form of constraint and cost functions, and discussed with respect to the results of the optimization. Only appropriate options for manned flight are considered, which yields three main conversion maneuvers. First, the initial altitude is maintained. Second, an upward motion of the aircraft can be exploited to have a positive effect on the AoA, thereby avoiding flow separation. The last option is the opposite and consequently includes a downward motion, which initially sounds counterintuitive, as that further increases the AoA.

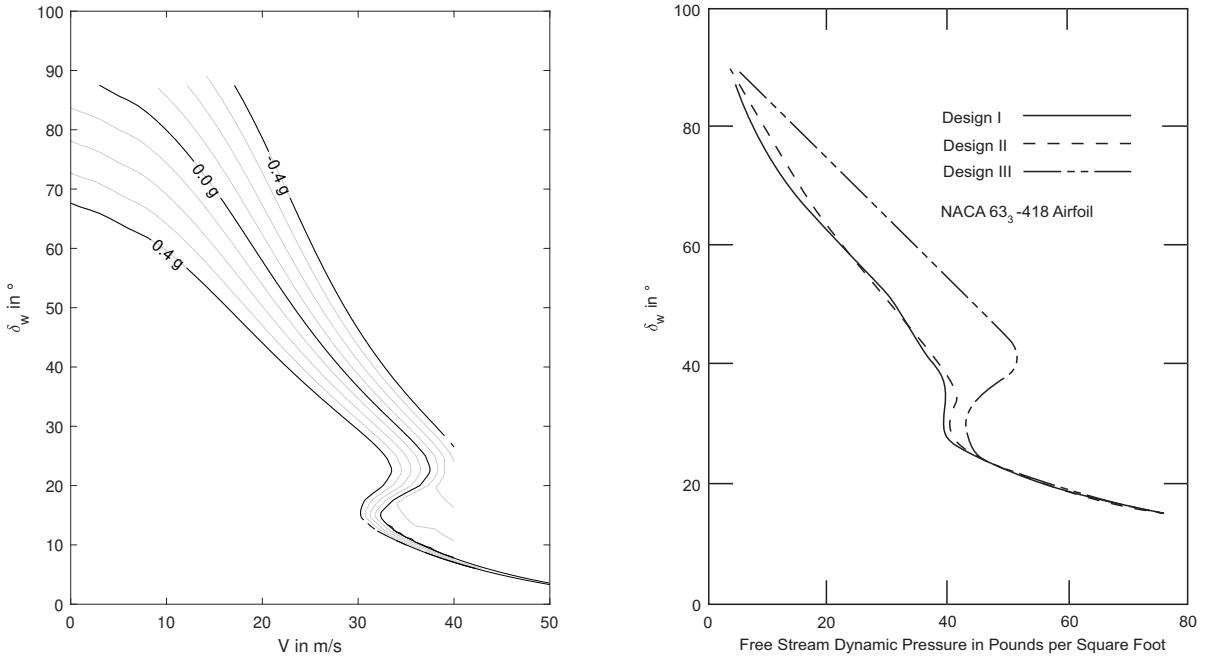

(a) Trajectories for different horizontal accelerations, from [9]

(b) Trim results for three different wing designs, according to [14]

Fig. 3 Comparison of transition trajectories with characteristic fold, for simulation-based tandem tilt-wing and wind-tunnel-based single wing trim studies.

A. Level Transition

The level transition maintains the initial altitude h throughout the maneuver, leading to $\dot{h} = 0$. It is a typical reference case for static trim analysis [13, 14]. Without a vertical velocity component, high effective AoA are usually encountered during the transition and flow separation occurs. This is more severe for re-transition maneuvers, as the thrust setting is low and the effect of the slipstream is small. The post-stall flight regime is characterized by its non-linearity, wherefore trim points are not unique when crossing the stall boundary, and the tilt angle trajectory takes the shape of an "S"-curve or fold. This effect has already been discovered in 1968 by Kirkpatrick and Murphy[14] in the course of static wind-tunnel investigations, and was reproduced independently in previous work [9] (compare Fig. 3) and by Cook[13] The occurrence of the fold in the tilt-angle range depends on the selected airfoil and its respective stall onset. It seems to force the aircraft to perform a deceleration in an accelerated conversion maneuver, and vice versa. This is not only counterintuitive, but also uncomfortable for pilot and passengers. According to [14], the effect can be reduced by deploying stall delaying airfoils or control surfaces acting like high-lift devices. Furthermore, the author in [14] mentions that the transition fold is not encountered or at least strongly decreased in the course of flight tests. That is primarily due to inertial effects in dynamic transitions, which were neglected in the trim studies. It is therefore interesting to see whether the same result can be obtained with the dynamic analysis using the optimal control approach.

Instead of strictly limiting the vertical motion by adapting variable and rate boundaries in Table 1, an upward motion ($0 \leq z^E$, $0 \leq \dot{z}^E$) is allowed in order to avoid too hard constraints for the optimization. Instead, the cost function is used

to enforce the level transition, with $w_2 = w_3 = w_4 = 0$ in Eq. (22). The reference altitude is replaced with the initial altitude z_0^E. The solver is capable to minimize the integral squared vertical displacement to the order of 10^{-7}. If only the vertical offset is considered as objective, longer transition times do not significantly impact the cost function, and the solution runs to the upper limit of the terminal time. Therefore, t_f is preserved in the cost function, but with $w_1 \ll w_4$.

$$J = w_1\, t_f + \int_0^{t_f} \left[w_4 \left(z^E - z_0^E \right)^2 \right] dt \tag{23}$$

Forward The resulting trajectory is shown in Fig. 4. In the upper plot, the black arrow represents the aerodynamic and propulsive force vector, which accelerates the vehicle in horizontal direction while balancing the gravitational vertical force. As can be seen, the initial and terminal force vectors are purely vertical with magnitude of the gravitational force, as these states are trimmed. In the second plot, arrows represent the attitude of both wings. In order to illustrate the offset between the two wing tilt angles, both arrows share the same origin in the vehicle's CG. While the canard tilt angle is higher in trimmed hover conditions (at $x = 0$), it passes the main wing's position in early transition and leads the transition maneuver, until the main wing tilt angle catches up in late transition. This is also visualized in Fig. 5(a). The behavior is due to the altered lever arms and their impact on the pitching moment as a function of tilt angle.

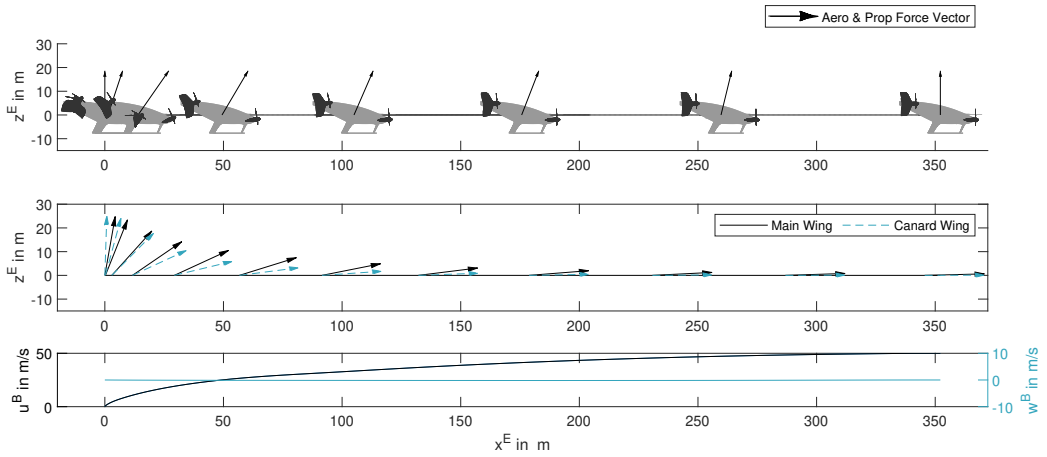

Fig. 4 Trajectory and velocities of level forward transition

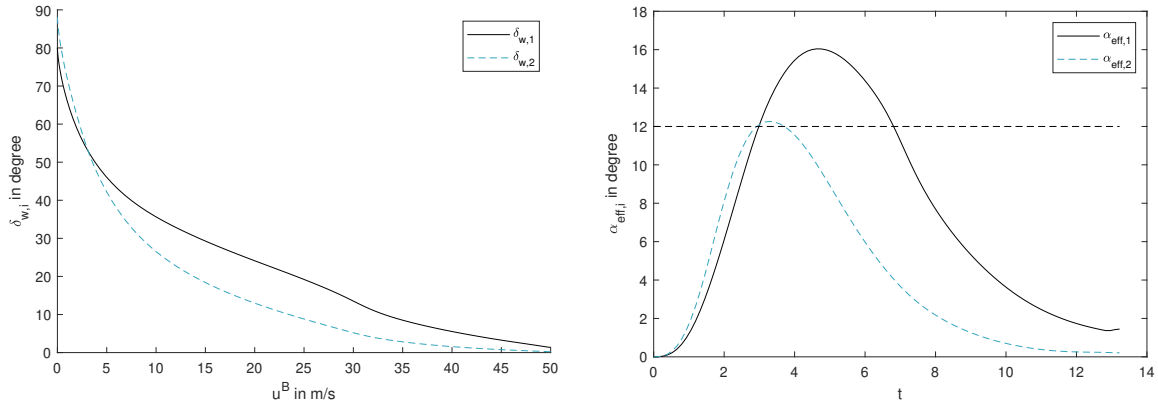

(a) Tilt angle trajectory

(b) Effective angles of attack

Fig. 5 Transition tilt angle trajectory and effective angles of attack for forward level transition.

The last plot shows the aircraft velocities in the body frame, which corresponds to the NED-frame for zero pitch. As intended, the vertical velocities are 0 while the horizontal velocity increases smoothly with ongoing transition.

As we were interested in the dynamic behavior in nonlinear post stall, the resulting transition trajectory is transferred to the same plot as in Fig. 3(a), where tilt angle is plotted over flight velocity. Fig. 5(a) shows that no transition fold as in the trim case is encountered. While there is a weak hump in $\delta_{w,1}$ at around 30°, $\delta_{w,2}$ stays smooth. The latter can be explained by Fig. 5(b), which shows that the canard wing does not encounter severe flow separation, as the maximum of $\alpha_{\text{eff},2}$ stays close to $\alpha_{\text{stall}} = 12°$ (indicated by the dashed horizontal line). That is due to a large thrust setting at the canard wing. In contrast, the main wing clearly crosses into the post-stall regime. Still, the fold occurring for trimmed flight is damped out. It was already shown in [6] that forward acceleration has a positive effect on the transition characteristics, wherefore the more meaningful analysis is on the backward transition. It shall be mentioned that the AoA for flow separation is a function of control surface deflection, but assumed to be constant in a first approach. Detailed results on all transition strategies can be found in the Appendix.

Backward Compared to the forward case, the solution for level backward transition covers a larger horizontal distance to perform the maneuver. [37] shows that deceleration capabilities of tilt-wings are limited. The relative motion of both tilt angles in Fig. 6 and Fig. 7(a) corresponds to the forward case. For low velocities $\delta_{w,2} < \delta_{w,1}$ holds, which is reverted for high velocities. As predicted by the trim analysis Fig. 3(a), negative accelerations push the tilt angle trajectories to higher values compared to the forward transition.

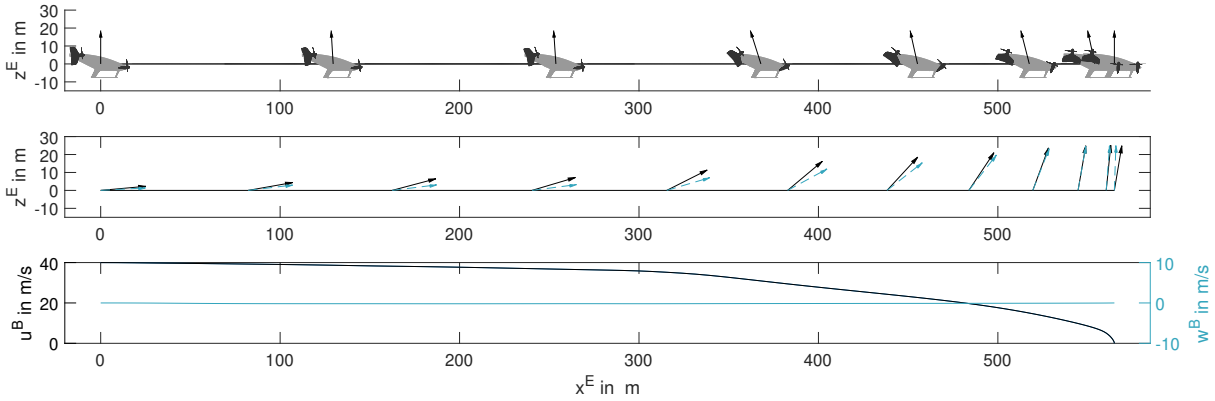

Fig. 6 Trajectory and velocities of level backward transition

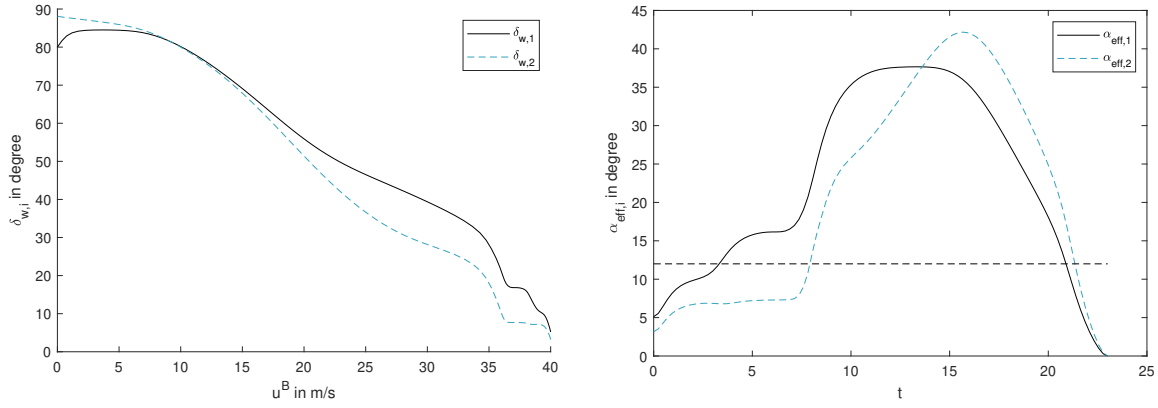

(a) Tilt angle trajectory

(b) Effective angles of attack

Fig. 7 Transition tilt angle trajectory and effective angles of attack for backward level transition.

The decelerating maneuver dictates low thrust settings, which result in larger effective AoA (compare Fig. 7(b). Consequently, both wings enter deeply into the post-stall region, which causes humps in the tilt angle trajectories during early re-transition. However, the curves for both tilt angles are still monotonous and a continuously decelerating

maneuver can be observed in the velocity plot. It is also apparent that deceleration capabilities are improved once the hump at $V = 35\,\mathrm{m\,s^{-1}}$ in Fig. 7(a), corresponding to $x^E \approx 300\,\mathrm{m}$ in Fig. 6, is passed.

B. In-/Outbound Transition

Depending on aircraft and airfoil, the onset of stall is often accompanied by large fluctuations (buffeting), while the resulting aerodynamic coefficients in [35] (used in Eq. (12)) represent an averaged result in this AoA range. Strong fluctuations of aerodynamic forces put stress on crew, passengers and aircraft structure, and might also have a negative effect on flight stability. Therefore, transformational aircraft often try to avoid flight in the post-stall regime [2] by loosening the vertical velocity constraint and performing so-called in-/outbound maneuvers [11]. Within the optimal control framework, path constraints for the effective AoA are introduced:

$$\alpha_{\mathrm{eff},i} < \alpha_{\mathrm{stall}} \tag{24}$$

The in- and outbound transition is usually based on an upward motion, which can be included in the constraints by restricting $\dot{z}^E$ to always be positive. It was already mentioned that a large increase of altitude during transition is undesired, especially for the backward case. For forward transition however, upward motion can be desired during transition to initiate the climb phase. Nevertheless, we gain more insight by focusing on the boundary case and therefore penalize the terminal altitude within the cost function for both forward and backward transition:

$$J = w_1\, t_f + w_3\, z_f^E \tag{25}$$

Outbound The results show that the aircraft is capable to satisfy both level and flow separation constraint, and the resulting trajectory for outbound transition looks similar to the results obtained for the level strategy in Fig. 6. It is therefore not shown. Instead, we are more interested in the differences between the two cases. For the level transition, the effective angles of attack are only moderately exceeding the stall boundary, so slight modifications of actuator inputs are sufficient to prevent flow separation.

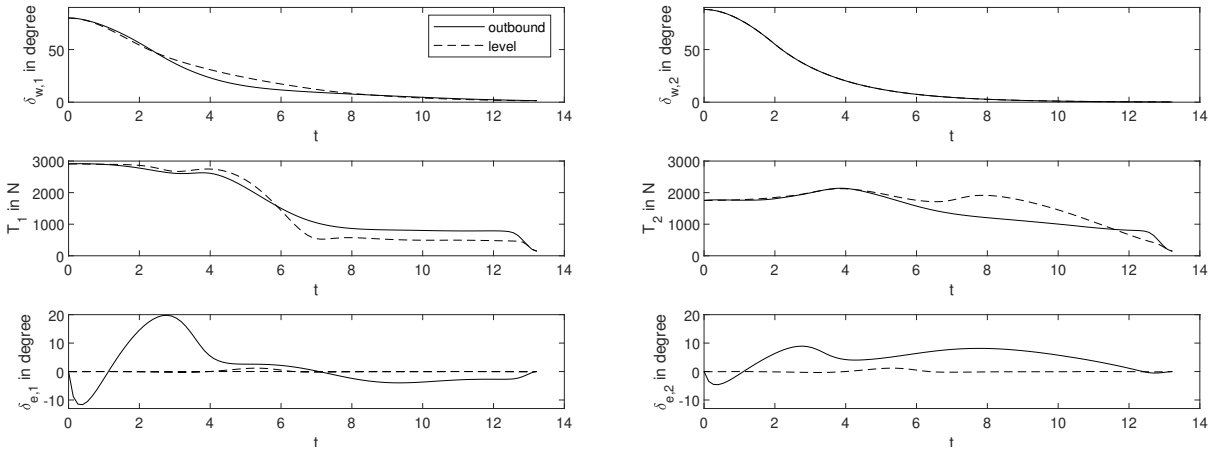

(a) Main Wing (b) Canard Wing

Fig. 8 Comparison of actuator inputs at both wings for outbound and level transition.

A comparison between outbound and level strategy is given for thrust and tilt angle in Fig. 8. While the canard tilt angle stays more or less unchanged, the main wing tilt angle is reduced within the time span from 3 to about 8 s, where stall occurred for the level maneuver (compare Fig. 5(b)), in order to reduce the effective AoA. A combination of control surface deflection and differential thrust compensates for the change in tilt angle. In comparison to the level case, where control surfaces are hardly deployed, large deflections are required especially on the main wing. Fig. 9 proofs that flow separation is successfully avoided, leading to a smoother tilt angle trajectory when compared to the level case.

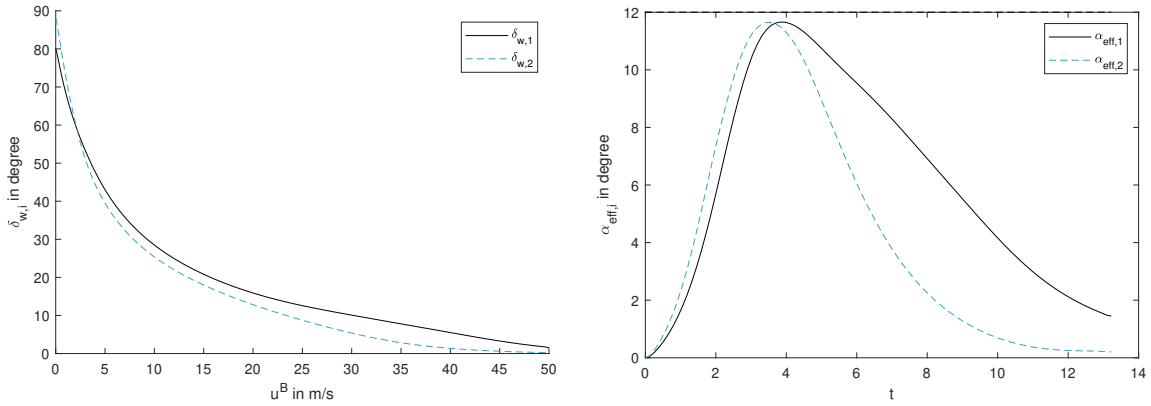

(a) Tilt angle trajectory (b) Effective angles of attack

Fig. 9 Transition tilt angle trajectory and effective angles of attack for outbound transition.

Inbound While a forward level transition was possible without flow separation, the inbound re-transition requires an upward motion to reduce the effective angle of attack, see Fig. 9. The conversion of kinetic to potential energy can be exploited to achieve short backward transitions when comparing final time and distance with the level case.

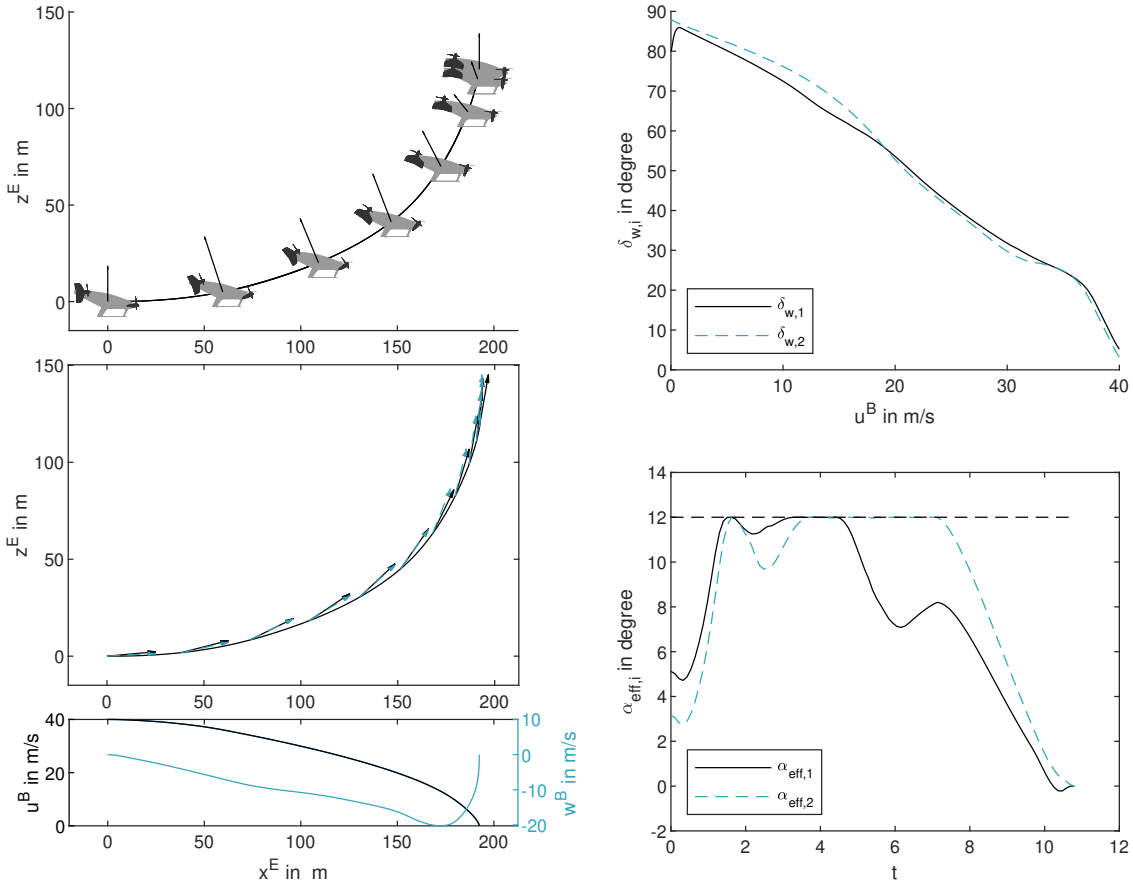

Fig. 10 Results for inbound transition.

The total aerodynamic and propulsive force acts as centripetal force that causes a circular upward motion, as shown

in the upper left plot in Fig. 10. In late re-transition, the force vector is tilted to the left, which leads to a strong deceleration of both upward (due to gravitation) and forward motion. The center left plot illustrates the idea behind in- and outbound transition. In order to reduce the effective AoA, the tilt angle deflection is kept almost tangential to the flight path. That explains why both tilt angle deflections take similar trajectories in the upper right plot until assuming the differential tilt configuration for trimmed hover flight at $u^B = 0$. Comparing this plot with the result for the level transition, the desired smoothing effect in the tilt angle trajectory is observed. The AoA plot in Fig. 10 proofs that flow separation is successfully avoided, leading to a smoother tilt angle trajectory when compared to the level case.

C. Dive & Glide Path Transition

The last subsection demonstrated that an upward motion can effectively reduce the AoA and avoid stall. Now, the opposite direction of the flight envelope shall be investigated and a downward motion is enforced during transition.

Dive Transition The dive transition exploits the conversion of potential to kinetic energy to quickly gain velocity in forward transition. A loss in altitude is accepted, wherefore the vertical force provided by airfoils and thrust is not required to balance gravity. From an optimal control perspective, the state boundaries in Table 1 are adapted to allow only a downward motion. It was already observed for the inbound maneuver that the shortest transitions can be achieved when exploiting energy conversion. To enforce a dive transition, the terminal time is set as single objective (similar results are obtained when minimizing the terminal distance).

$$J = w_1 \, t_f \tag{26}$$

As shown in in Fig. 11, the cost function successfully triggers the desired behavior, and the aircraft descends more than 80 m throughout the maneuver. Without having to create sufficient lift to balance gravitation, the aircraft is allowed to rapidly tilt both wings downwards. This results in a large acceleration in both downward and forward direction. With rising flight speed, aerodynamic forces become dominant and the aircraft quickly transitions from thrust- to wing-borne flight. As expected, the dive trajectory results in a severe increase of effective AoA.

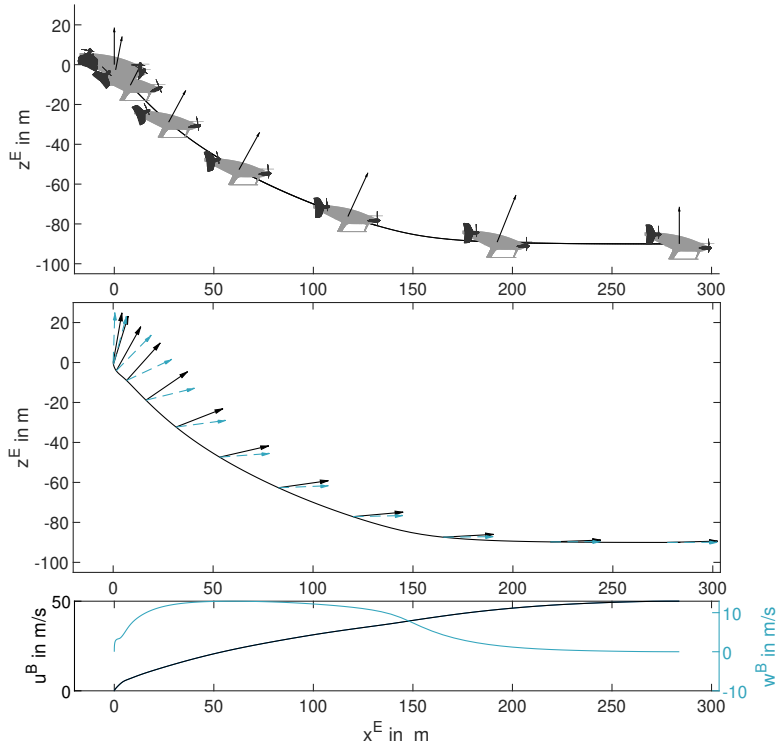

Fig. 11 Trajectory and velocities of dive transition

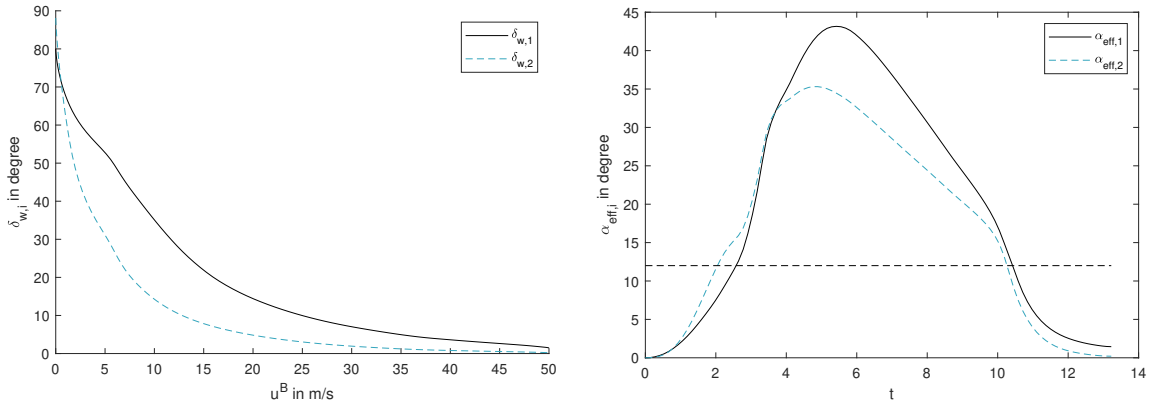

(a) Tilt angle trajectory

(b) Effective angles of attack

Fig. 12 Transition tilt angle trajectory and effective angles of attack for dive transition.

Glide Path Conventional aircraft follow a glide path when approaching the runway. In order to reflect possible ATC requirements, a similar operation is considered in the form of the glide path transition. It shall be mentioned that this is the most challenging maneuver for common tilt-wing flight, as already stated by Michaelsen and Martin in 1963. Not only does the downward motion increase the AoA, while at the same time the propellers are close to idle (in order to allow deceleration) which reduces the positive slipstream effect on the effective AoA. In addition, the conversion of potential to kinetic energy along the glide path counteracts the desired decelerating maneuver. The strategy can be imposed by penalising deviation from a commanded glide path, represented by reference altitude z^E_{ref} in the cost function:

$$J = \int_0^{t_f} w_4 \left(z^E - z^E_{\text{ref}} \right)^2 dt \tag{27}$$

where the reference altitude is a function of the current horizontal position:

$$z^E_{ref} = z^E_0 - \left(x^E - \Delta x^E \right) \cdot \tan \gamma \tag{28}$$

with initial altitude z^E_0 and glide path angle γ. The "fade-in" distance Δx^E allows the aircraft to intercept the glide slope. Here, $\Delta x^E = 500\,\text{m}$, $z^E_0 = 100\,\text{m}$ and $\gamma = 15°$ were chosen. Although aircraft approaches are usually conducted at angles of about 3°, the high value for the path angle was chosen for better visualization of the trajectory (and because the vehicle allows to fly such a maneuver). To avoid climbing within the fade-in distance, an upward motion of the aircraft is restricted by variable constraints.

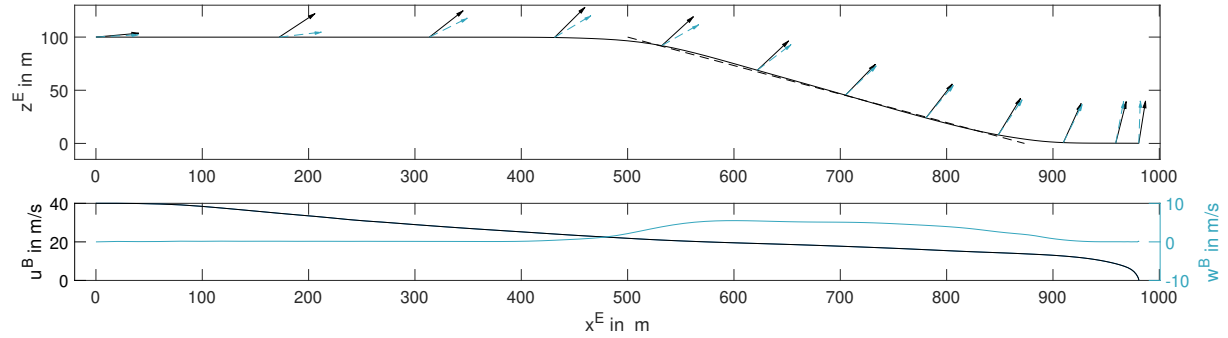

Fig. 13 Trajectory and velocities of glide path transition

Aiming at good tracking of the prescribed path, the influence of time on the objective is canceled by choosing $w_4 = 1/t_f$. Otherwise, the solution rather tries to minimize the flight time instead of accurately tracking the glide path.

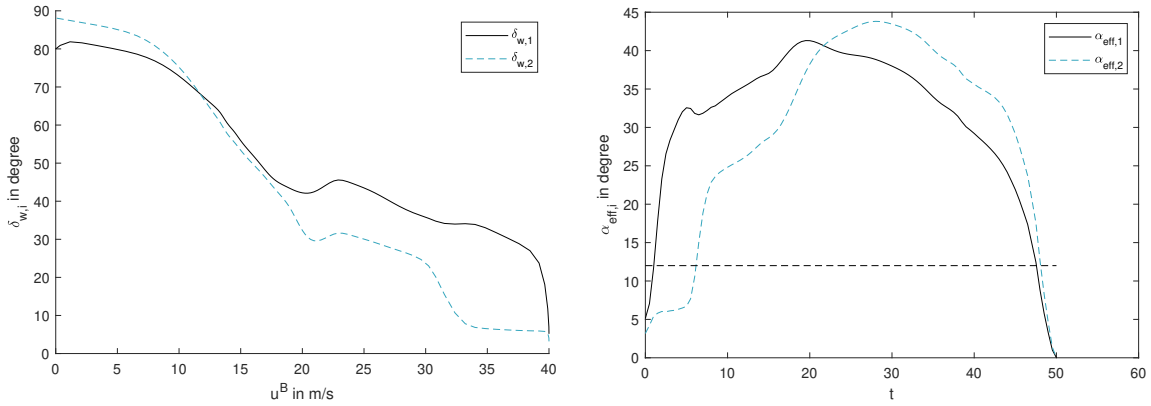

(a) Tilt angle trajectory

(b) Effective angles of attack

Fig. 14 Transition tilt angle trajectory and effective angles of attack for glide path transition.

The resulting trajectory is shown in Fig. 14, with the glide path being represented by a dashed line. It is interesting to see that a strong deceleration is initiated by an upward motion of the main wing within the fade-in distance. In this flight regime, both tilt angles do not show monotonous behavior and have a large offset. Fading into the glide slope, the aircraft already reduced its velocity by a factor of 2. On the glide path, both tilt wing deflections align, and the aircraft is still capable to decelerate horizontally. However, the gradient of u^B is smaller on the glide path compared to the fade-in distance. Section III.C confirms that this maneuver is undesirable from an aerodynamics point of view, as both wings are in post-stall throughout the transition.

IV. Discussion

With the ambition to investigate different regions of the transition corridor of tilt-wing aircraft, three different transition strategies were applied, which chiefly distinguish in the vertical motion of the aircraft.

The results confirm the findings of Michaelsen and Martin that the static phenomena of transition folds, as described in [13] and [2], are damped within a dynamic analysis. Furthermore, the investigations confirm that the re-transition maneuver is more challenging from a flight physics perspective. That is because of limited deceleration capabilities, low thrust settings and therefore weak slipstream effects on the effective angle of attack. While the forward transition can successfully avoid flow separation under level flight constraints, an upward motion is required to avoid stall in the re-transition. This is counterintuitive for landing approaches, where the intention is to descend. With respect to the trajectories of both tilt angles over horizontal flight speed, the results agree with the static findings in [13]. For decelerated backward transition maneuvers, the trajectories are pushed to the upper right, which corresponds to high tilt angles throughout the maneuver. The contrary is observed for forward transition maneuvers. This behavior further increases the effective angles of attack in re-transition. Sticking with the tilt angle trajectories, all presented transitions have in common that the canard tilt angle is lower than the main wing deflection for most part of the transition, excluding close-to-hover conditions. Accordingly, forward transitions are initiated primarily by a deflection of the canard wing, whereas backward transitions are led by deflections of the main wing. This becomes especially obvious for dive and glide path transition.

V. Conclusion

As a foundation for the determination of the transition corridor for tilt-wing aircraft, this paper presented a dynamic analysis of different transition strategies within an optimal control framework. The setup allows to find solutions for different constraints and objective functions, and the convergence is quite robust with respect to the initial guess solution, wherefore a complex generation of initial solutions can be avoided. The observed behavior under different transition strategies, for example with respect to tilt angle deflections and stall onset, corresponds to expectations and findings found in reference literature.

Next to minor improvements of the current optimal control framework, future work will be focused on the determination of the tilt-wing transition corridor. The corridor is defined by multiple constraints originating from

actuator saturation, structural limits, as well as handling quality and passenger comfort limits. Often, the transition corridor also includes a flow separation boundary. It is, therefore, intended to investigate the nature of post-stall buffeting in order to determine whether flight in post-stall is generally admissible or should be avoided. For that, an aerodynamic test campaign will be conducted on a scaled tilt-wing demonstrator. Next to insights on fluctuating behavior in flow separation, efforts will also be made to validate the strip theory model presented in a former work, which was the baseline for the reduced aerodynamic model used within the optimization presented in this paper.

Appendix

A. Results Level Forward Transition

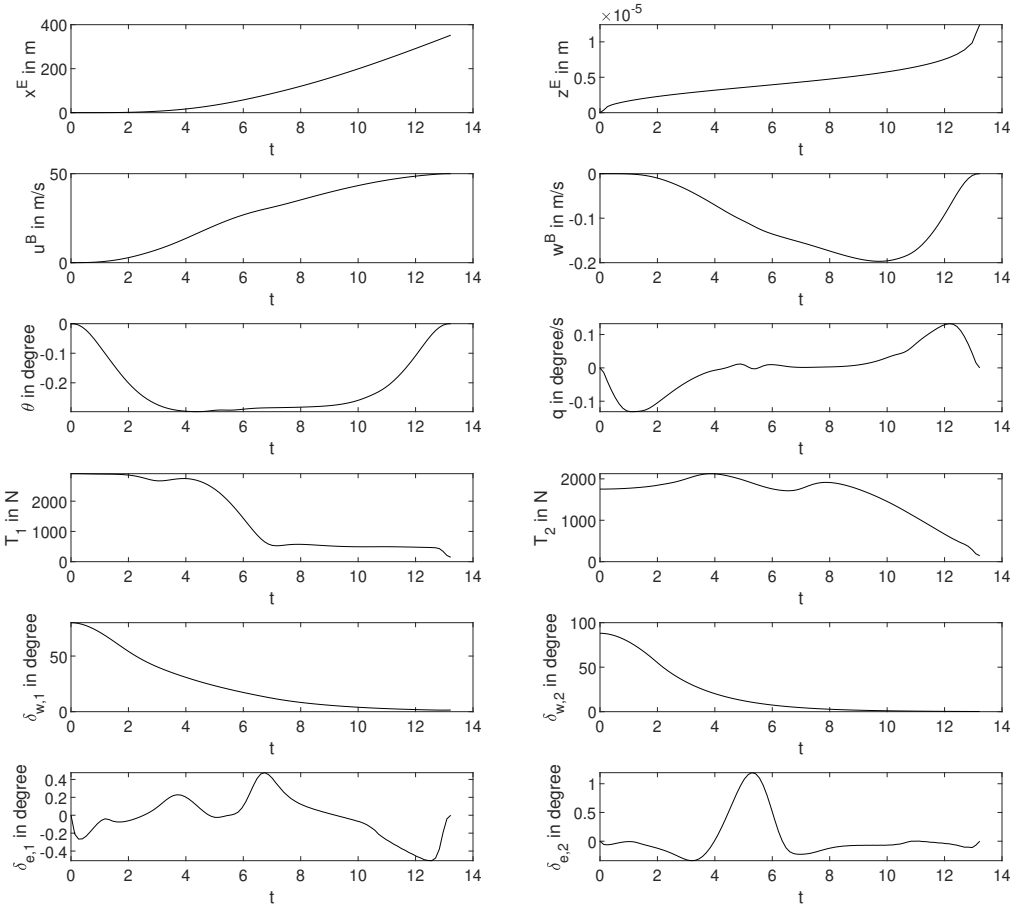

Fig. 15 States and inputs for level forward transition.

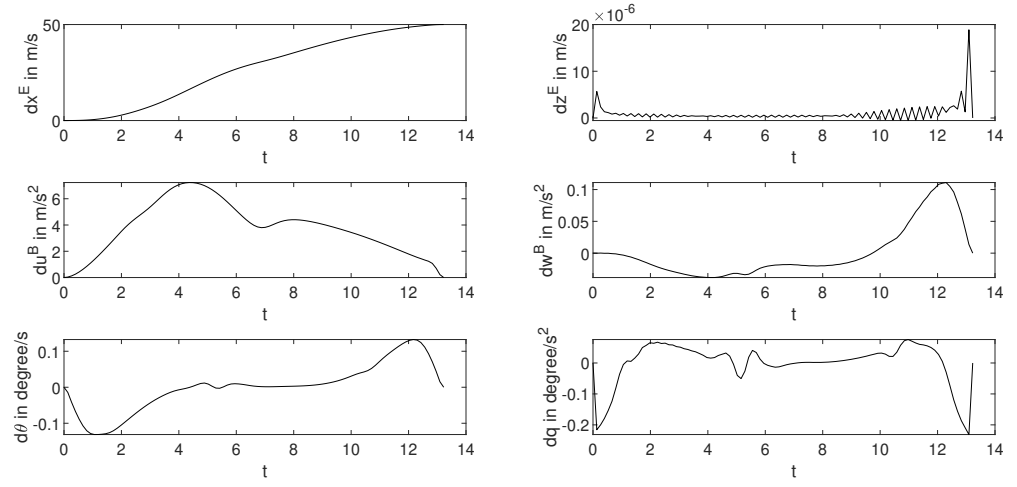

Fig. 16 State derivatives for level forward transition.

B. Results Level Backward Transition

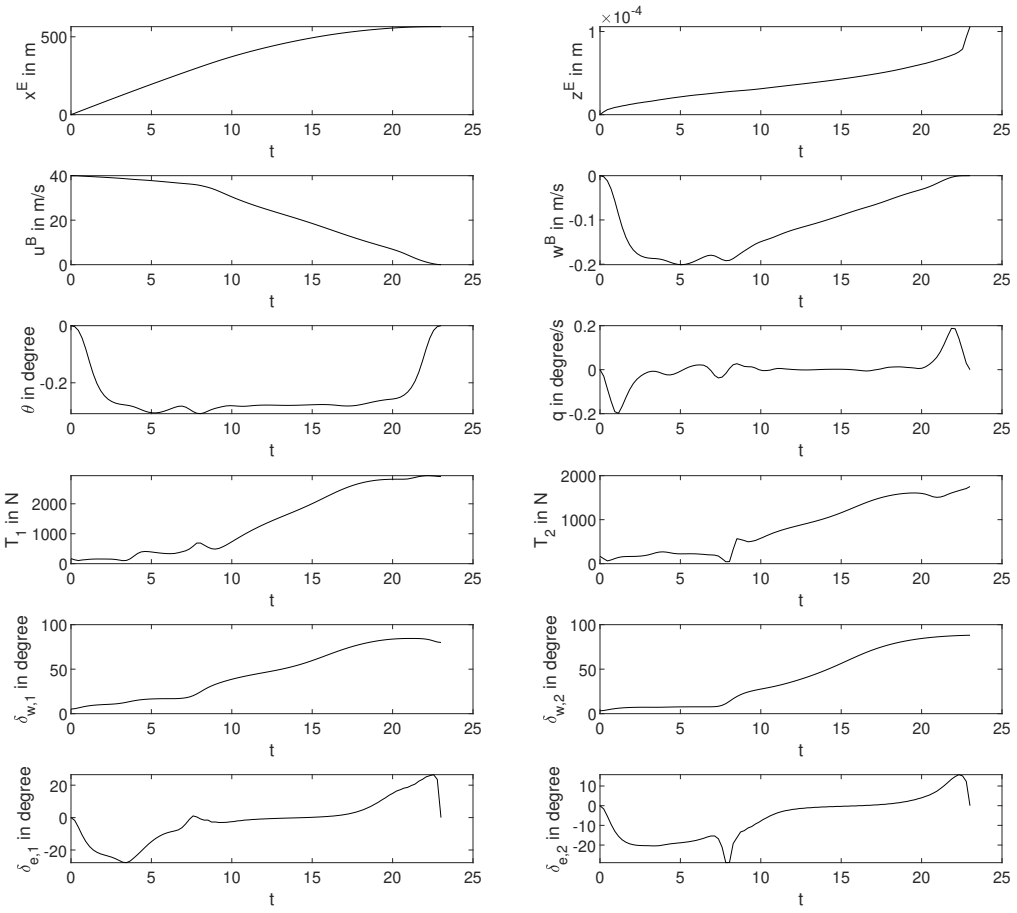

Fig. 17 States and inputs for level backward transition.

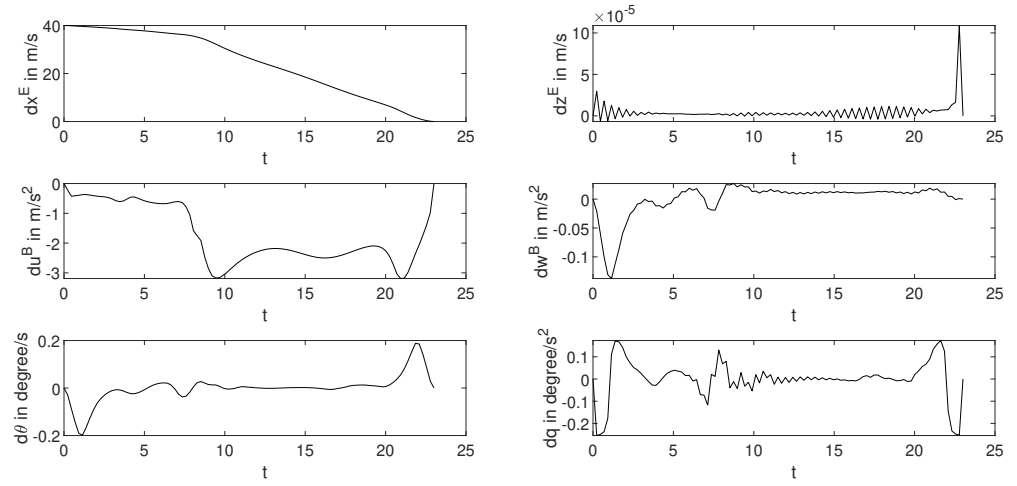

Fig. 18 State derivatives for level backward transition.

C. Results Outbound Transition

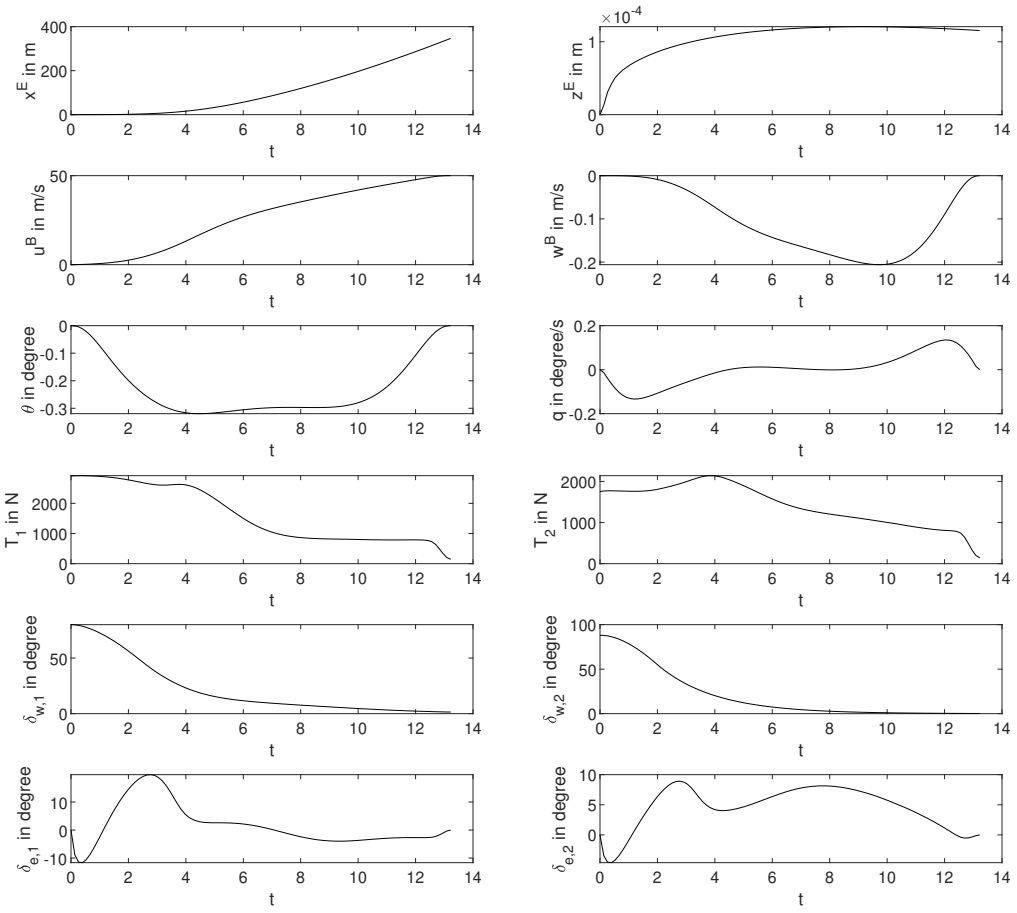

Fig. 19 States and inputs for outbound transition.

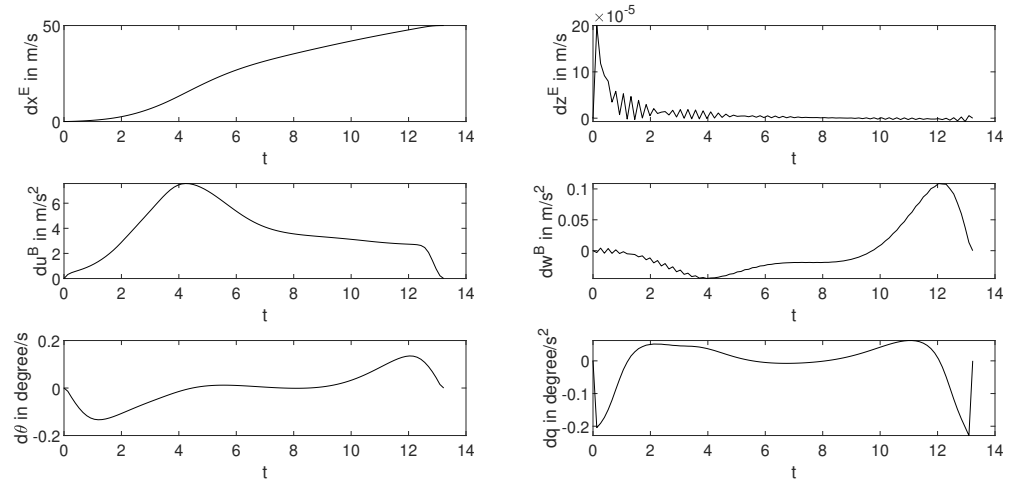

Fig. 20 State derivatives for outbound transition.

D. Results Inbound Transition

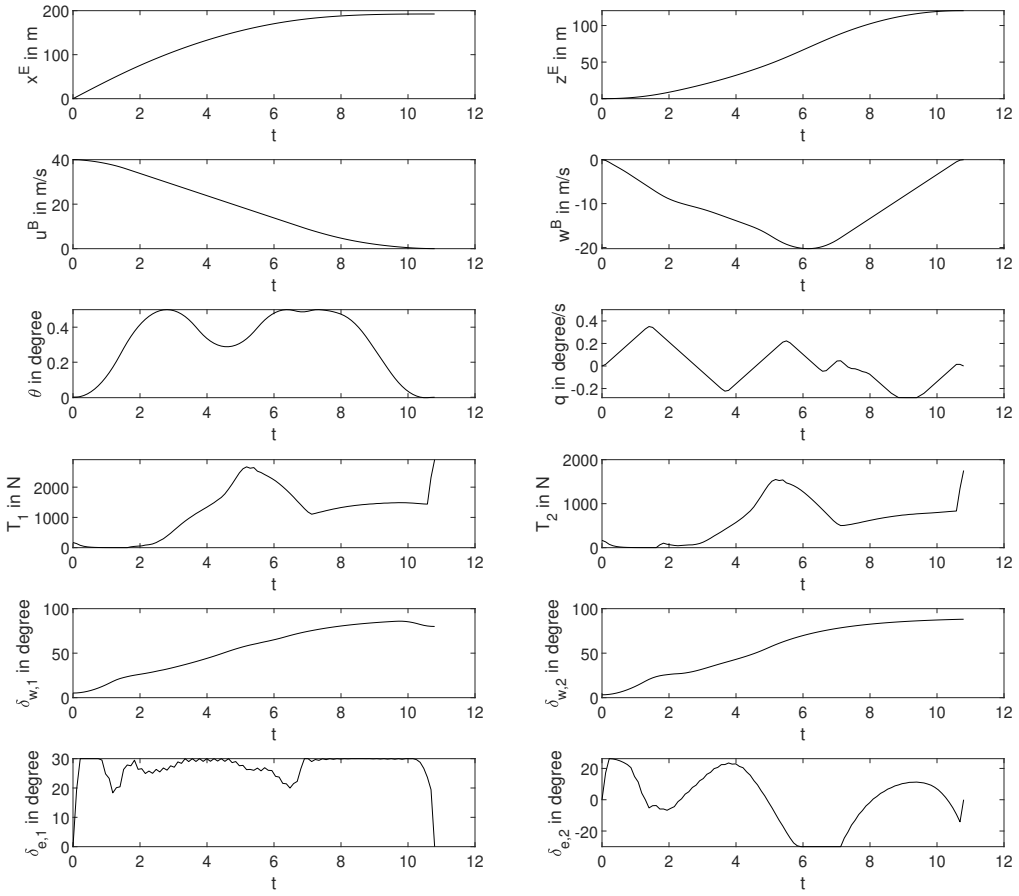

Fig. 21 States and inputs for inbound transition.

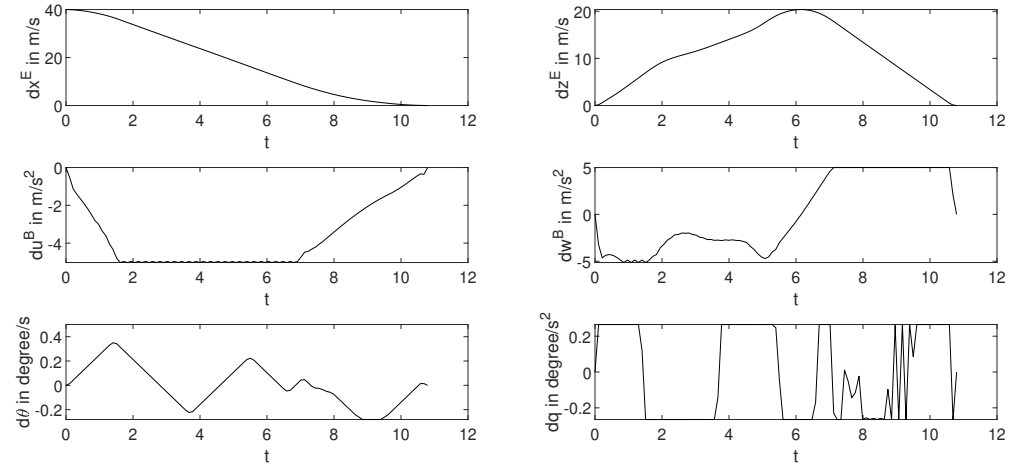

Fig. 22 State derivatives for inbound transition.

E. Results Dive Transition

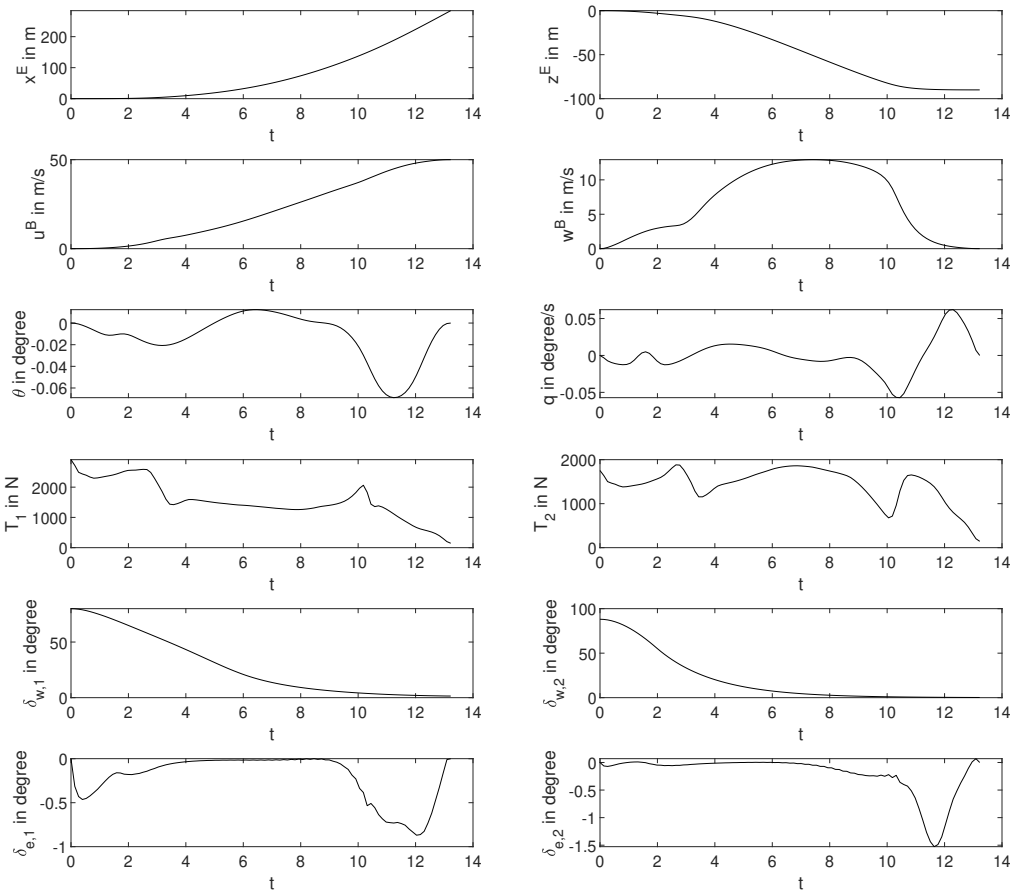

Fig. 23 States and inputs for dive transition.

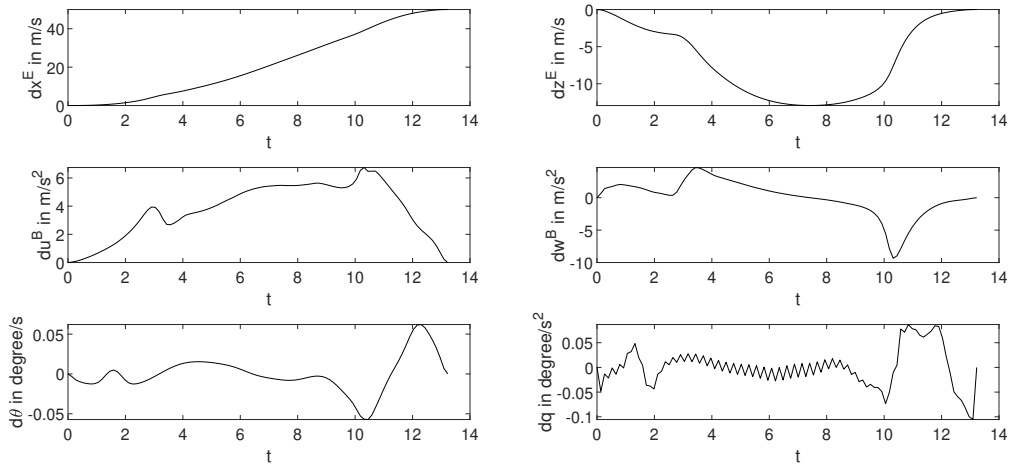

Fig. 24 State derivatives for dive transition.

F. Results Glide Path Transition

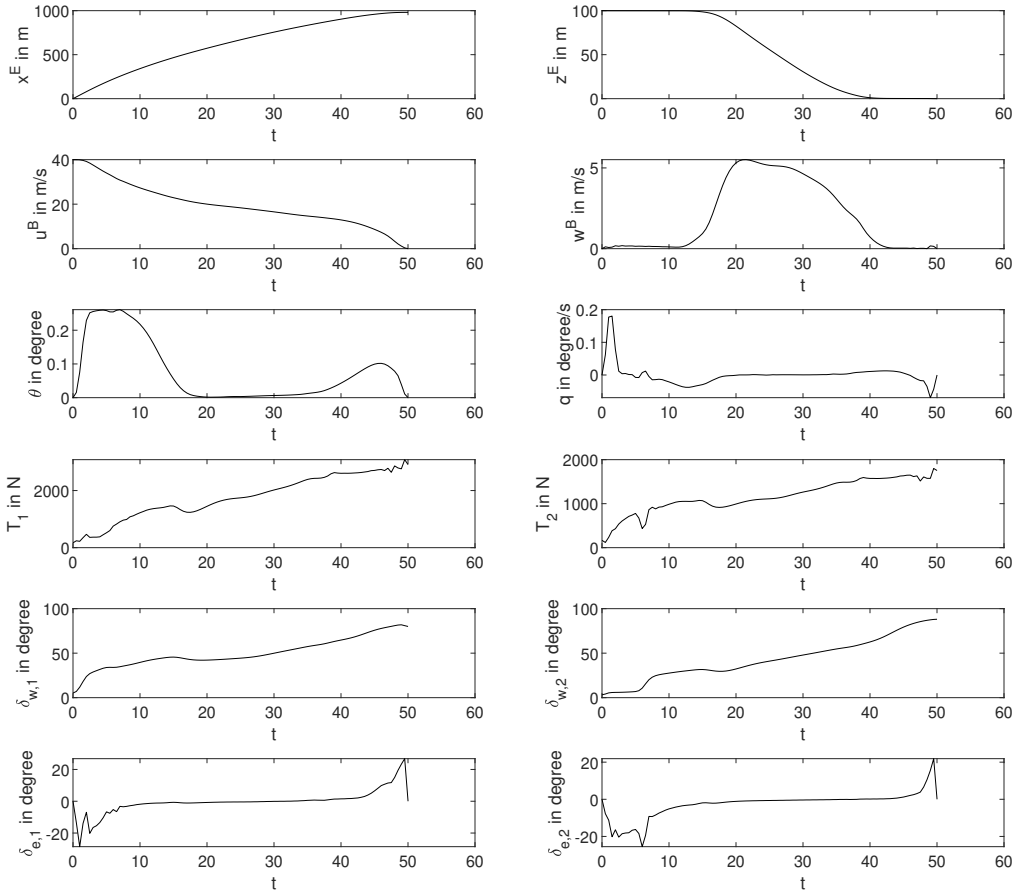

Fig. 25 States and inputs for glide path transition.

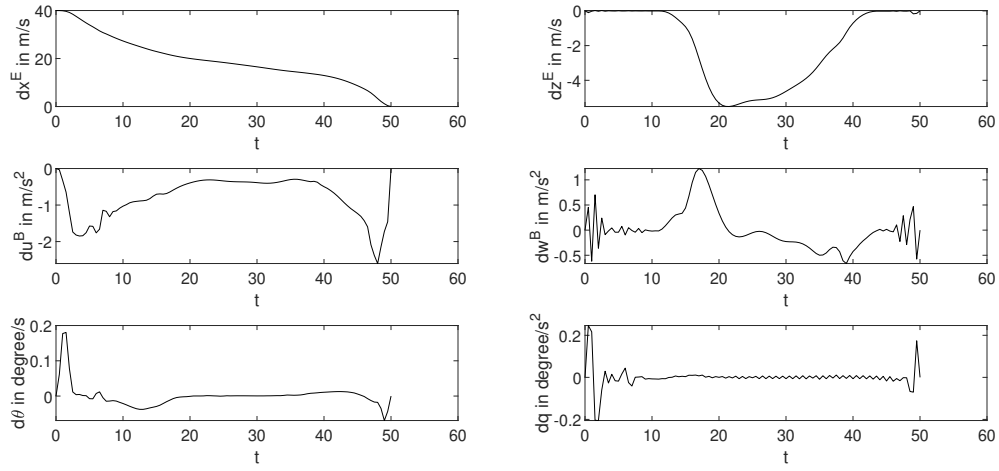

Fig. 26 State derivatives for glide path transition.

References

[1] Phillips, F. C., "The Canadair CL-84 Tilt-Wing V/STOL Programme," *The Aeronautical Journal*, Vol. 73, No. 704, 1969, pp. 713–723. https://doi.org/10.1017/S0001924000052003.

[2] Michaelsen, O. E., and Martin, J. F., "The Aerodynamic Approach to Improve Flying Qualities of Tilt-Wing Aircraft," *9th Anglo-American Aeronautical Conference*, 1963. https://doi.org/10.2514/6.1963-484.

[3] Breul, H. T., "A Simulator Study of Tilt-Wing Handling Qualities," *Heterogeneous Combustion Conference*, American Institute of Aeronautics and Astronautics, 1963. https://doi.org/10.2514/6.1963-1015.

[4] Josephs, L. C., and Hesse, W. J., "Survey of significant technical problems unique to VSTOL encounteredin the development of the XC-142A," *Journal of Aircraft*, Vol. 3, No. 1, 1966, pp. 3–10. https://doi.org/10.2514/3.43699.

[5] GAEBE, H. M., "Some important design considerations on the xc- 142a triservice vstol," *Journal of Aircraft*, Vol. 2, No. 1, 1965, pp. 9–12. https://doi.org/10.2514/3.43611.

[6] Cook, J., and Hauser, J., "A Strip Theory Approach to Dynamic Modeling of eVTOL Aircraft," *AIAA Scitech 2021 Forum*, 2021. https://doi.org/10.2514/6.2021-1720.

[7] Milz, D., and Looye, G., "Tilt-Wing Control Design for a Unified Control Concept," *AIAA SCITECH 2022 Forum*, 2022. https://doi.org/10.2514/6.2022-1084.

[8] Binz, F., Islam, T., and Moormann, D., "Attitude control of tiltwing aircraft usinga wing-fixed coordinate system andincremental nonlinear dynamic inversion," *International Journal of Micro Air Vehicles*, Vol. 1, 2019, pp. 1–12.

[9] May, M., Milz, D., and Looye, G., "Semi-Empirical Aerodynamic Modeling Approach for TandemTilt-Wing eVTOL Control Design Applications," *AIAA SCITECH 2023 Forum*, 2023.

[10] Deckert, W. H., Page, R. V., and Dickinson, S. O., "Large-scale Wind-tunnel Tests of Descent Performance of an Airplane Model with a Tilt Wing and Differential Propeller Thrust," Tech. rep., NASA, 1964.

[11] Fredericks, W. J., McSwain, R. G., Beaton, B. F., and Klassman, D. F., "Greased Lightning (GL-10) Flight Testing Campaign," , 2017.

[12] Rubin, F., "Modelling & Analysis of a Tilt Wing Aircraft," Master's thesis, KTH, Royal Institute of Technology Stockholm, Schweden, 2018.

[13] Cook, J. W., "Exploration of Dynamic Transitions of Tiltwing Aircraftusing Differential Geometry," Ph.D. thesis, University of Colorado, 2022.

[14] Kirkpatrick, D. G., and Murphy, R. D., "Planning Wind-Tunnel Test Programs for V/STOL Conversion Studies," *AIAA 3rd Aerodynamic Testing Conference*, 1968.

[15] Hartmann, P., Meyer, C., and Moormann, D., "Unified Velocity Control and Flight State Transitionof Unmanned Tilt-Wing Aircraft," *Journal of Guidance, Control, and Dynamics*, Vol. 40, No. 6, 2017, pp. 1348–1359.

[16] Lu, Z., Hong, H., Gerdts, M., and Holzapfel, F., "Flight Envelope Prediction via OptimalControl-Based Reachability Analysis," *Journal of Guidance, Control, and Dynamics*, Vol. 45, No. 1, 2022, pp. 185–195.

[17] Nabi, H. N., Lombaerts, T., Zhang, Y., and van Kampen, E., "Effects of Structural Failure on the Safe Flight Envelope of Aircraft," *Journal of Guidance, Control, and Dynamics*, Vol. 41, No. 6, 2018, pp. 1257–1275.

[18] Betts, J. T., *Practical Methodsfor Optimal Controland Estimation UsingNonlinear Programming - Second Edition*, SIAM, 2010.

[19] Doff-Sotta, M., Cannon, M., and Bacic, M., "Fast optimal trajectory generation for a tiltwing VTOL aircraft with application to urban air mobility," *2022 American Control Conference (ACC)*, Unpublished, 2022, pp. 1–6. https://doi.org/10.13140/RG.2.2.20119.50080, URL http://rgdoi.net/10.13140/RG.2.2.20119.50080.

[20] Chauhan, S. S., and Martins, J. R. R. A., "Tilt-Wing eVTOL Takeoff Trajectory Optimization," *Journal of Aircraft*, Vol. 57, No. 1, 2020, pp. 93–112. https://doi.org/10.2514/1.C035476.

[21] Panish, L., and Bacic, M., "Transition Trajectory Optimization for a Tiltwing VTOLAircraft with Leading-Edge Fluid Injection Active Flow Control," *AIAA SCITECH Forum 2022*, 2022.

[22] Li, B., Sun, J., Zhou, W., Wen, C.-Y., Low, K. H., and Chen, C.-K., "Transition Optimization for a VTOLTail-Sitter UAV," *IEEE/ASME Transactions on Mechatronics*, Vol. 25, No. 5, 2020, pp. 2534–2545.

[23] Kubo, D., and Suzuki, S., "Tail-Sitter Vertical Takeoff and Landing Unmanned AerialVehicle: Transitional Flight Analysis," *Journal of Aircraft*, Vol. 45, No. 1, 2008, pp. 292–297.

[24] Oosedo, A., Abiko, S., Konno, A., and Uchiyama, M., "Optimal transition from hovering to level-flight of a quadrotortail-sitter UAV," *Auton Robot*, Vol. 41, 2016, pp. 1143–1159.

[25] McIntosh, K., Reddinger, J.-P., Zhao, D., and Mishra, S., "Optimal Trajectory Generation for Transitioning Quadrotor Biplane TailsitterUsing Differential Flatness," *Vertical Flight Society's 77th Annual Forum & Technology Display*, 2021.

[26] Tal, E., Ryou, G., and Karaman, S., "Aerobatic Trajectory Generation for a VTOL Fixed-Wing Aircraft Using Differential Flatness," , 2022.

[27] Yang, Y., Zhu, J., Wang, X., Yuan, X., and Zhang, X., "Dynamic Transition Corridors and Control Strategy ofa Rotor-Blown-Wing Tail-Sitter," *Journal of Guidance, Control and Dynamics*, Vol. 44, No. 10, 2021, pp. 1836–1852.

[28] Zhong, J., and Wang, C., "Transition characteristics for a small tail-sitterunmanned aerial vehicle," *Chinese Journal of Aeronautics*, 2021.

[29] Rieck, R. M., "Discrete Controls and Constraints in Optimal Control Problems," Ph.D. thesis, Technische Universität München, 2017.

[30] Nie, Y., Faqir, O., and Kerrigan, E. C., "ICLOCS2: Try this Optimal Control Problem Solver Before you Try the Rest," *2018 UKACC 12th International Conference on Control (CONTROL)*, IEEE, 2018. https://doi.org/10.1109/control.2018.8516795.

[31] Wächter, A., and Biegler, L. T., "On the implementation of an interior-point filter line-search algorithm for large-scale nonlinear programming," *Mathematical Programming*, Vol. 106, No. 1, 2005, pp. 25–57. https://doi.org/10.1007/s10107-004-0559-y.

[32] May, M. S., Looye, G., and Milz, D., "Dynamic Modeling and Analysis of Tilt-Wing Electric Vertical Take-Off and Landing Vehicles," *AIAA SCITECH 2022 Forum*, 2022. https://doi.org/10.2514/6.2022-0263.

[33] Leishman, J. G., *Principles of Helicopter Aerodynamics*, Cambridge University Press, 2000.

[34] McCormick, B. W., *Aerodynamics of V/STOL flight*, dover ed ed., Dover Publications, Mineola, N.Y, 1999. Includes bibliographical references and index.

[35] Montgomerie, B., *Methods for Root Effects, Tip Effects and Extending the Angle of Attack Range to +- 180°, with Application to Aerodynamics for Blades on Wind Turbines and Propellers*, Swedish Defence Research Agency, Stockholm, 2004.

[36] Olson, E. D., "Semi-Empirical Prediction of Aircraft Low-Speed Aerodynamic Characteristics," *53rd AIAA Aerospace Sciences Meeting*, 2015. https://doi.org/10.2514/6.2015-1679.

[37] Milz, D., May, M., and Looye, G., "Dynamic Inversion-Based Control Concept for Transformational Tilt-Wing eVTOLs," *AIAA SCITECH 2024 Forum*, 2024.